DYNAMICS OF VARIANTS OF TWO-DIMENSIONAL CANTILEVERED THIN FLEXIBLE PLATES IN AXIAL FLOW

Liaosha Tang
University of Toronto Institute for Aerospace Studies, Toronto, Canada
Michael P. Païdoussis
Department of Mechanical Engineering, McGill University, Montreal, Canada
Jin Jiang
School of Power and Mechanical Engineering, Wuhan University, Wuhan, P.R.China

ABSTRACT

Cantilevered thin flexible plates in subsonic axial flow may lose stability at sufficiently high flow velocity. Once the critical point is exceeded, flutter takes place, and the flutter amplitude grows as the flow velocity further increases. One can observe rich dynamics from this fluid-structure interaction system when some variants are taken into account. In particular, this paper considers two cases: with (i) a spring support of either linear or cubic type, and (ii) a concentrated mass mounted on the plate. For each specific variant of the original system, the influence of the "additional" spring support or concentrated mass is investigated in terms of its magnitude as well as location. Some interesting phenomena found in the dynamics of the variants of the system are summarized in this paper.

1. INTRODUCTION

The dynamics of cantilevered thin flexible plates in axial flow is one the classical problems of applied mechanics. Some of the early work was concerned with the flapping of flags (see Kornecki (1978)) and the dynamics of aircraft and missile skins, particularly in supersonic flow (Dowell, 1975). More recently, there has been renewed interest in the dynamics of cantilevered, typically long, plates in incompressible flow, not only as an abstract problem, but also for engineering applications, e.g., in paper-making (Watanabe et al., 2002), for electricity generation (Allen and Smits, 2001), and in biomimesis (Triantafyllou et al., 2004).

The present paper summarizes some recent researches conducted by the authors on this topic. The two-dimensional plate is modelled as a beam with an inextensible centreline, and an unsteady lumped vortex model is used to calculate the pressure difference across the oscillating plate. The analysis of the system dynamics is carried out in the time-domain. The system loses stability by flutter at sufficiently high flow velocity, and both the instability threshold, as a function of the system parameters, and the post-critical behaviour of the system have recently been studied extensively by Tang and Païdoussis (2007). Two variants of the system are studied in the present paper: in the presence of (i) a spring support, linear or nonlinear, somewhere along the plate, and (ii) a concentrated mass, at various locations along the length of the plate. The current research has not only originated from theoretical curiosity but is also related to the design of a new type energy-harvesting device, which is presented in another paper.

2. THE ORIGINAL SYSTEM

A schematic diagram of a cantilevered flexible plate in axial flow is shown in Fig. 1. The geometrical characteristics of the rectangular homogeneous plate are the length of the flexible section L, width B and thickness h; $B \to \infty$ and $h \ll L$ for a two-dimensional thin plate. Normally, there is a rigid segment of length L_0 as part of the clamping arrangement at the upstream end. The other physical parameters of the system are: the plate material density $\rho_{\rm P}$ and bending stiffness $D = Eh^3/\sqrt{12(1-\nu^2)}$, where E and ν are, respectively, Young's modulus and the Poisson ratio of the plate material, the fluid density $\rho_{\rm P}$, and the undisturbed flow velocity U. As shown in Fig. 1, W and V are, respectively, the transverse and longitudinal displacements of the plate. $F_{\rm L}$ and $F_{\rm D}$ are the aero/hydro-dynamic loads acting on the plate in the transverse and longitudinal directions, respectively. S is the distance of a material point on the plate from the origin,

measured along the plate centreline in a coordinate system embedded in the plate. Moreover, material damping of the Kelvin-Voigt model is considered, with the loss factor denoted by a.

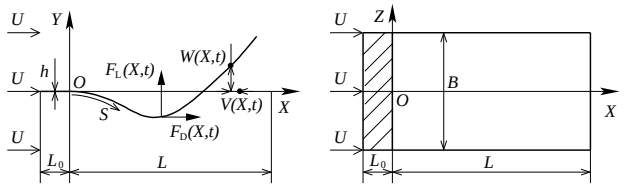

Figure 1: A cantilevered flexible in axial flow.

The equations of motion of the plate can be written in nondimensional form as (Tang and Païdoussis, 2007)

$$\begin{aligned} & \ddot{w} + \left(1 + \alpha \frac{\partial}{\partial \tau}\right) \\ \times \quad & \left[w'''' \left(1 + w'^2\right) + 4w'w''w''' + w''^3\right] \\ + \quad & w' \int_0^s \left(\dot{w}'^2 + w'\ddot{w}'\right)\, ds \\ - \quad & w'' \int_s^1 \left[\int_0^s \left(\dot{w}'^2 + w'\ddot{w}'\right)\, ds\right]\, ds = f_{\text{eff}}, \end{aligned} \tag{1}$$

$$v = -\frac{1}{2}\int_0^s w'^2\, ds, \tag{2}$$

$$f_{\text{eff}} = \mu {U_{\text{R}}}^2 \left(f_{\text{L}} - w' f_{\text{D}} + w'' \int_s^1 f_{\text{D}}\, ds\right), \tag{3}$$

where the overdot and the prime represent $\partial(\,)/\partial\tau$ and $\partial(\,)/\partial s$, respectively. The nondimensional variables are defined by

$$\begin{aligned} & (x, y) = \frac{(X, Y)}{L},\ (w, v) = \frac{(W, V)}{L},\ s = \frac{S}{L}, \\ & \tau = \frac{t}{\sqrt{\rho_{\text{P}} h L^4/D}},\ \alpha = \frac{a}{\sqrt{\rho_{\text{P}} h L^4/D}}, \\ & l_0 = \frac{L_0}{L},\ f_{\text{L}} = \frac{F_{\text{L}}}{\rho_{\text{F}} U^2},\ f_{\text{D}} = \frac{F_{\text{D}}}{\rho_{\text{F}} U^2}. \end{aligned} \tag{4}$$

Moreover, the mass ratio μ and the reduced flow velocity U_{R} are, respectively, defined by

$$\mu = \frac{\rho_{\text{F}} L}{\rho_{\text{P}} h}, \quad U_{\text{R}} = UL\sqrt{\frac{\rho_{\text{P}} h}{D}}. \tag{5}$$

In Eq. (3), the aero/hydro-dynamic loads are calculated using the unsteady lumped vortex model (Tang and Païdoussis, 2007). On each individual panel, the pressure difference across the plate Δp is first computed and then decomposed into the *lift* f_{L} and the *drag* f_{D}. That is

$$f_{\text{L}i} = \Delta p_i \cos\alpha_i, \quad f_{\text{D}i} = \Delta p_i \sin\alpha_i + C_{\text{D}}, \tag{6}$$

where α_i is the incidence angle of the ith panel. And an additional drag coefficient C_{D}, assuming a uniform distribution over the whole length of the plate, may be considered in f_{D} to account for the viscous effects of the fluid flow.

The analytical model of the original system is first validated against available experimental data for the flutter threshold, and it has been shown that the level of agreement is superior to that achieved by other theories (Tang and Païdoussis, 2007), though still not sufficiently good – with theory generally under-predicting the threshold. This discrepancy between theoretical predictions and experimental observations has been attributed to the lack of a proper accounting of (viscous) aero/hydro-dynamic drag in the theory, which would increase the tension in the plate and thus the stability threshold of the system. Another prominent "weakness" of all theories, including ours, is that they fail to predict the subcritical bifurcation and strong hysteresis observed in the experiments. One possible explanation may be that all experiments are conducted in a wind or water tunnel, while all theories normally consider open flow. However, the reason causing the observed subcritical bifurcation may be very complicated (see the work by Tang and Païdoussis (2007) for details); the exact underlying mechanism is still an open question.

As already shown in the work by Tang and Païdoussis (2007) for a specific system with $\mu = 0.2$, the dynamics of the system without springs or masses added is relatively simple. When U_{R} is below the critical point U_{Rc}, the plate remains straight; any small disturbance to the system is attenuated. Once U_{R} exceeds U_{Rc}, flutter occurs, and the flutter amplitude grows as U_{R} increases further.

3. WITH AN ADDITIONAL SPRING SUPPORT

A schematic diagram of a cantilevered flexible plate with an additional (linear or cubic) spring support in axial flow is shown in Fig. 2, where S_{S} is the location of the spring, $F_{\text{S}} = -K_{\text{L}} W(S_{\text{S}}) - K_{\text{C}} W(S_{\text{S}})^3$ is the spring force acting on the plate, and K_{L} and K_{C} are the stiffnesses of the linear or cubic spring, as the case may be. When the vibration amplitude is large, the longitudinal displacement of the plate, V, becomes important.

In the present paper, the additional spring support is assumed to be able to move longitudinally with the plate; only transverse spring forces are considered. Therefore, the equations of motion of the plate are still given by Eqs. (1) and (2). However, instead of Eq. (3), the effective force acting on the plate should be calculated by

$$f_{\text{eff}} = \mu {U_{\text{R}}}^2 \left(f_{\text{L}} - w' f_{\text{D}} + w'' \int_s^1 f_{\text{D}}\, ds \right) + f_{\text{S}} \delta(s - s_{\text{S}}), \tag{7}$$

where δ denotes the Dirac delta function, and $s_{\text{S}} = S_{\text{S}}/L$ is the location of the additional spring support normalized by the length of the flexible plate L. The nondimensional spring force f_{S} is given by

$$f_{\text{S}} = \frac{L^3}{D} F_{\text{S}} = -k_{\text{L}} w - k_{\text{C}} w^3, \tag{8}$$

where k_{L} and k_{C} are, respectively, the nondimensional stiffnesses of the linear and the cubic spring, defined by

$$k_{\text{L}} = \frac{L^4}{D} K_{\text{L}}, \qquad k_{\text{C}} = \frac{L^6}{D} K_{\text{C}}, \tag{9}$$

which represent the ratios of the spring forces to the restoring force of the plate.

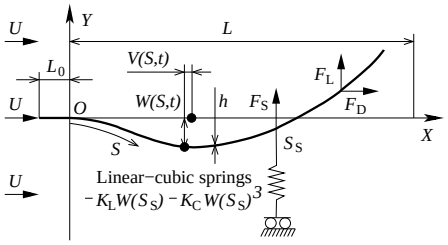

Figure 2: A cantilevered flexible plate with an additional spring support in axial flow.

When a linear spring support is added, the plate may lose stability statically (buckling or divergence instability) rather than by flutter. Stability diagrams of a cantilevered flexible plate in axial flow with an additional linear spring support at $s_{\text{S}} = 1$ and $s_{\text{S}} = 0.8$ are shown in Figs. 3 and 4, respectively. It is found that the system dynamics is dependent not only on the stiffness but also on the location of the spring.

When the linear spring support is located at $s_{\text{S}} = 1$, it can be seen in Fig. 3 that the plate loses stability through flutter at various values of U_{R}, provided $k_{\text{L}} < 59$; loss of stability through

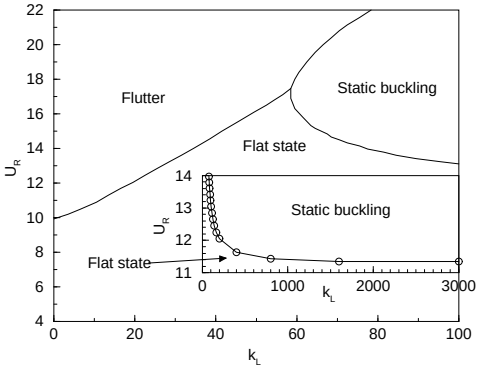

Figure 3: Stability diagram of a cantilevered flexible plate in axial flow with an additional linear spring support at the plate trailing edge, i.e., $s_{\text{S}} = 1$. The system parameters are: $\mu = 0.2$, $l_0 = 0.01$, $\alpha = 0.004$ and $C_{\text{D}} = 0$. The spring force is given by $f_{\text{S}} = -k_{\text{L}} w(s = 1)$.

divergence (buckling) occurs when $k_{\text{L}} > 59$. For $k_{\text{L}} < 59$, the value of U_{Rc} increases with increasing k_{L}. On the other hand, when $k_{\text{L}} > 59$, U_{Rc} decreases as k_{L} increases. However, with further increase in k_{L}, U_{Rc} converges to a constant $U_{\text{Rc}} = 11.30$, as shown in the inset of Fig. 3. This implies that a clamped/simply-supported plate in axial will lose stability through buckling at $U_{\text{Rc}} = 11.30$ for the particular values of μ, l_0, α and C_{D} used in the calculations (see the caption of Fig. 3), since the linear spring support is equivalent to a simple support when $k_{\text{L}} \to \infty$. Moreover, when $k_{\text{L}} > 59$, the plate may develop flutter at higher values of U_{R}, beyond the onset of buckling. It can be shown that all the limit cycle oscillations observed in the flutter region of Fig. 3 are of the symmetric type. At a given value of k_{L}, the flutter amplitude grows with increasing U_{R}. The plate cannot develop divergence (buckling) again, beyond the flutter threshold in this range of k_{L}.

As shown in Fig. 4, the three stable states (i.e., stable flat state, static buckling and flutter) can also be seen when $s_{\text{S}} = 0.8$. The plate loses stability through flutter when $k_{\text{L}} < 193$. For a range of k_{L} around $k_{\text{L}} = 193$, divergence may succeed flutter at higher U_{R}. But, when $k_{\text{L}} > 193$, the primary instability is buckling; flutter never takes place, no matter how large U_{R} is. Again, only symmetric limit cycle oscillations are found in the flutter region; at a fixed value of k_{L}, the flutter amplitude grows as U_{R} increases. A very interesting stronger-constraint/less-stable phenomenon that can be observed in Fig. 4: the

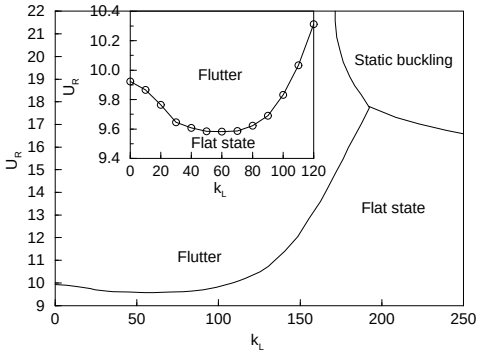

Figure 4: Stability diagram of a cantilevered flexible plate in axial flow with an additional linear spring support at $s_{\rm S} = 0.8$. The system parameters are: $\mu = 0.2$, $l_0 = 0.01$, $\alpha = 0.004$ and $C_{\rm D} = 0$. The spring force is given by $f_{\rm S} = -k_{\rm L} w(s = 0.8)$.

system loses stability at a lower critical reduced flow velocity $U_{\rm Rc}$ when $0 < k_{\rm L} < 106$ than when $k_{\rm L} = 0$. In fact, when $0 < k_{\rm L} < 56$, the value of $U_{\rm Rc}$ *decreases* as $k_{\rm L}$ increases.

If the additional spring support is cubic, it can be seen in Fig. 5 for the case $s_{\rm S} = 0.8$ and $k_{\rm C} = 6000$ that the system exhibits richer dynamics. The system still loses stability through flutter, but in a very abrupt manner, at $U_{\rm Rc} = 9.92$. After the primary bifurcation, the system develops symmetric limit cycle oscillations, before a secondary bifurcation takes place at $U_{\rm R} = 15.33$; beyond this point, the limit cycle oscillations become asymmetric. In the region of period-1 asymmetric limit cycle oscillation (i.e., $15.33 < U_{\rm R} < 17.86$), it is interesting to see that, with increasing $U_{\rm R}$, the flutter amplitude of the plate trailing edge decreases. A series of period-doubling bifurcations take place at $U_{\rm R} = 17.86$, 18.49 and 18.74. A region of chaotic motions occurs when $18.81 < U_{\rm R} < 19.62$. However, as $U_{\rm R}$ is increased further, regular limit cycle oscillations re-emerge; another period doubling route to chaos can be observed in the region $19.62 < U_{\rm R} < 21.10$. The main region of chaos is for $21.10 < U_{\rm R} < 23.45$; there is a periodic window between $U_{\rm R} = 22.36$ and $U_{\rm R} = 22.56$. Finally, the plate becomes statically buckled when $U_{\rm R} > 23.45$.

4. WITH AN ADDITIONAL CONCENTRATED MASS

When there is an additional concentrated mass $m_{\rm A}$ located at $S_{\rm M}$ on the plate, as illustrated in

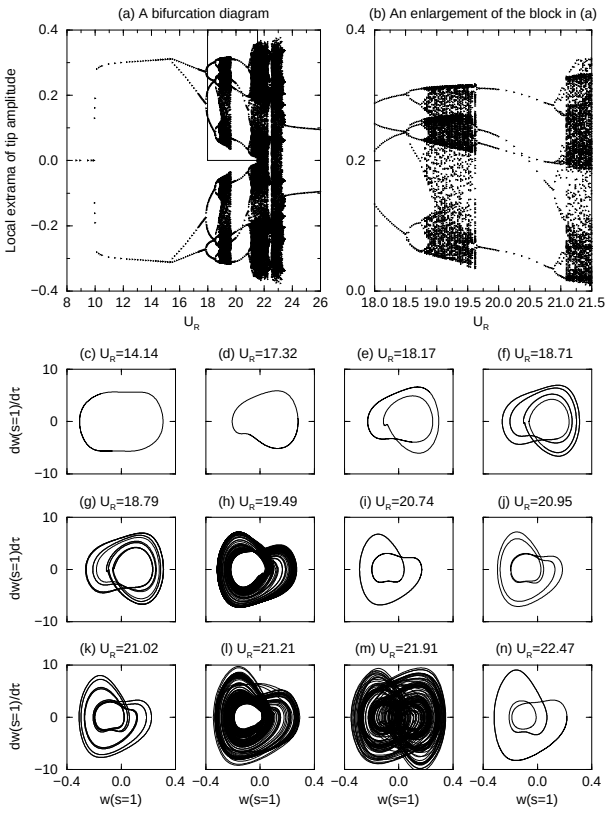

Figure 5: The dynamics of a cantilevered flexible plate in axial flow with an additional cubic spring support at $s_{\rm S} = 0.8$. The system parameters are: $\mu = 0.2$, $l_0 = 0.01$, $\alpha = 0.004$ and $C_{\rm D} = 0$. The spring force is given by $f_{\rm S} = -k_{\rm C} w^3(s = 0.8)$, where $k_{\rm C} = 6000$.

Fig. 6, the equation of motion of the plate, i.e., Eq. (1), should be rewritten as

$$\begin{aligned} & \left[1 + \sigma_{\rm M}\delta(s - s_{\rm M})\right] \ddot{w} + (1 + \alpha \frac{\partial}{\partial \tau}) \\ \times \quad & \left[w'''' \left(1 + w'^2\right) + 4w'w''w''' + w''^3\right] \\ + \quad & \left[1 + \sigma_{\rm M}\delta(s - s_{\rm M})\right] w' \int_0^s \left(\dot{w}'^2 + w'\ddot{w}'\right) ds \\ - \quad & w'' \int_s^1 \left[1 + \sigma_{\rm M}\delta(s - s_{\rm M})\right] \\ \times \quad & \left[\int_0^s \left(\dot{w}'^2 + w'\ddot{w}'\right) ds\right] ds = f_{\rm eff}, \end{aligned} \tag{10}$$

where δ denotes the Dirac delta function, and the mass parameter $\sigma_{\rm M}$ is defined by

$$\sigma_{\rm M} = \frac{m_{\rm A}}{\rho_{\rm P} h L}, \tag{11}$$

representing the ratio of the additional concentrated mass to the mass of the plate itself (in

the sense of the per-unit-width mass). Moreover, $s_{\rm M}$ is the location of the additional concentrated mass, normalized by the length of the flexible plate L, i.e., $s_{\rm M} = S_{\rm M}/L$.

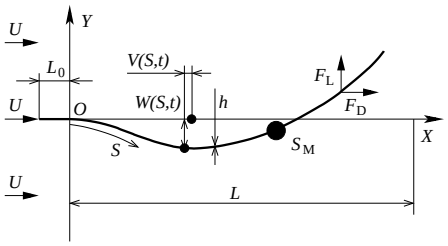

Figure 6: A cantilevered flexible plate in axial flow with an additional concentrated mass.

The influence of an additional concentrated mass, for various values of $\sigma_{\rm M}$ and $s_{\rm M}$ on stability is shown in Fig. 7.

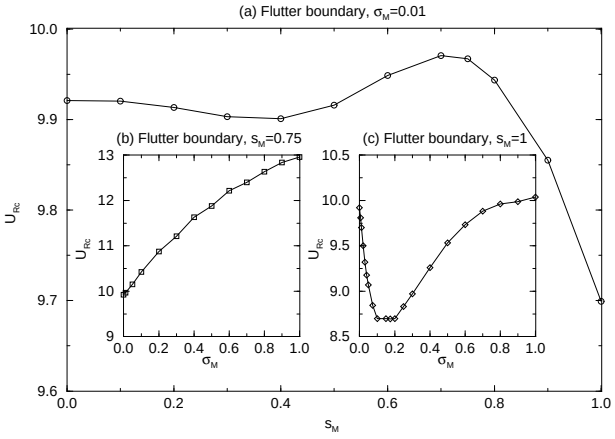

Figure 7: The influence of an additional concentrated mass on system stability. The other parameters of this system are $\mu = 0.2$, $l_0 = 0.01$, $\alpha = 0.004$ and $C_{\rm D} = 0$.

It can be seen in Fig. 7(a) that a small additional concentrated mass $\sigma_{\rm M} = 0.01$ at a variety of locations along the length of the plate has different effects on the critical point. When there is no additional mass, i.e., for $s_{\rm M} = 0$, $U_{\rm Rc} = 9.92$. When $s_{\rm M} < 0.4$, the value of $U_{\rm Rc}$ decreases slightly with increasing $s_{\rm M}$. When $0.4 < s_{\rm M} < 0.7$, $U_{\rm Rc}$ grows with increasing values of $s_{\rm M}$ and reaches the maximum $U_{\rm Rc} = 9.97$ at $s_{\rm M} = 0.7$. Beyond this maximum point, $U_{\rm Rc}$ decreases again, more rapidly this time, as $s_{\rm M}$ further increases; finally, the minimum $U_{\rm Rc} = 9.70$ is observed when the additional concentrated mass is located at the trailing edge of the plate, i.e., $s_{\rm M} = 1$.

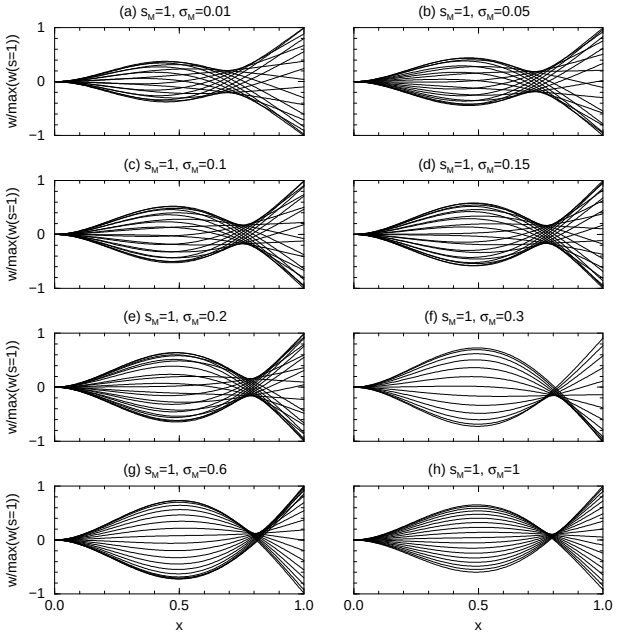

Figure 8: The vibration modes of the systems with various additional concentrated masses located at the trailing edge of the plate, i.e., $s_{\rm M} = 1$. Note that the vibrations modes are obtained at the corresponding critical point of each individual case. The other parameters of the system are $\mu = 0.2$, $l_0 = 0.01$, $\alpha = 0.004$ and $C_{\rm D} = 0$.

When $s_{\rm M} = 0.75$ or $s_{\rm M} = 1$ while $\sigma_{\rm M}$ is varied, the flutter boundaries obtained are, respectively, shown in Figs. 7(b) and (c). It can be seen in Fig. 7(b) that, when $s_{\rm M} = 0.75$, the value of $U_{\rm Rc}$ increases monotonically from $U_{\rm Rc} = 9.92$ with $\sigma_{\rm M} = 0$ to $U_{\rm Rc} = 12.96$ with $\sigma_{\rm M} = 1$. When $s_{\rm M} = 1$, the relation between $U_{\rm Rc}$ and $\sigma_{\rm M}$ becomes complicated: as shown in Fig. 7(c), $U_{\rm Rc}$ decreases significantly with increasing $\sigma_{\rm M}$ when $0 < \sigma_{\rm M} < 0.1$; however, for $0.1 < \sigma_{\rm M} < 0.2$, the variation in $U_{\rm Rc}$ is negligibly small, and a plateau is formed where $U_{\rm Rc} = 8.70$. As $\sigma_{\rm M}$ is increased further, the trend for $U_{\rm Rc}$ is reversed; and, finally $U_{\rm Rc} = 10.04$ when $\sigma_{\rm M} = 1$. The pattern of the flutter boundary presented in Fig. 7(c) may be correlated to the vibration modes of the plate along the flutter boundary, as shown in Fig. 8. One can find that, when $\sigma_{\rm M}$ is small, say $\sigma_{\rm M} < 0.2$, the mode shapes of the plate in Figs. 8(a) through (e) are qualitatively the same; these vibration modes are combinations of the first and second beam-mode shapes. In contrast, when $\sigma_{\rm M} \geq 0.3$, as shown in Figs. 8(f) through (h), the vibration modes are solely determined by the second-beam-mode shape, in that a quasi-

stationary node becomes more prominent.

It has been observed in Fig. 7(a) that a small additional concentrated mass $\sigma_{\mathrm{M}} = 0.01$ located at $s_{\mathrm{M}} = 1$ significantly reduces the value of critical point; moreover, as shown in Fig. 9, it also affects the manner of the onset of the flutter and the post-critical dynamics of the system. It is seen in Fig. 9(a) that, as compared to the bifurcation diagram of the system in the original configuration, flutter takes place in a more abrupt manner; and, beyond the critical point, the flutter amplitude is rather large. This phenomenon may imply the occurrence of a subcritical bifurcation instead of a supercritical one.

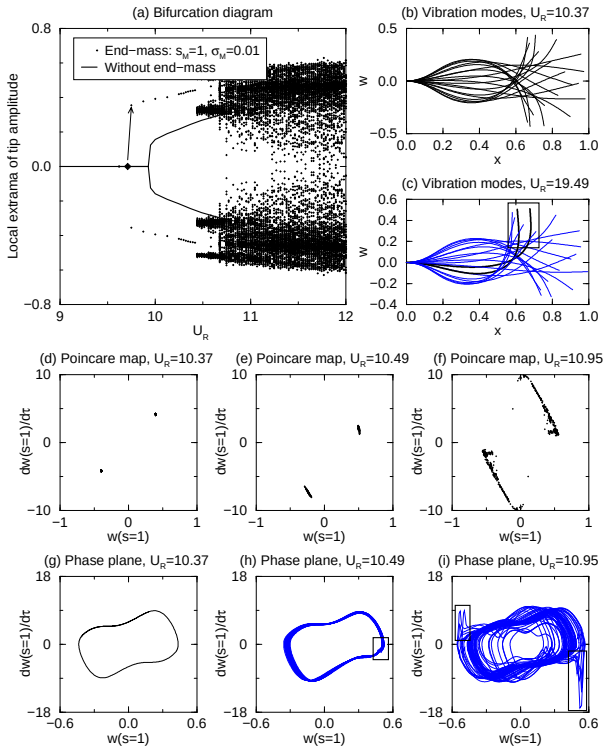

Figure 9: The dynamics of the system with a small concentrated mass located at the trailing edge of the plate, i.e., $\sigma_{\mathrm{M}} = 0.01$ and $s_{\mathrm{M}} = 1$. The other parameters of the system are $\mu = 0.2$, $l_0 = 0.01$, $\alpha = 0.004$ and $C_{\mathrm{D}} = 0$. Note that the Poincaré maps are obtained by simultaneously recording the position and the velocity of the trailing edge of the plate with $w(s = 0.5) = 0$ as the controlling event.

With the small additional concentrated mass $\sigma_{\mathrm{M}} = 0.01$ located at $s_{\mathrm{M}} = 1$, symmetric limit cycle oscillations can still be observed at higher U_{R} beyond the critical point $U_{\mathrm{Rc}} = 9.70$, as shown in Figs. 9(b), (d) and (g) for the case $U_{\mathrm{R}} = 10.37$ for example. Note that the flutter amplitude of the system with an additional mass is significantly larger than that of the system in the original configuration, even though $\sigma_{\mathrm{M}} = 0.01$ is so small. As U_{R} increases further and exceeds $U_{\mathrm{R}} = 10.43$, chaos takes place, as shown in Figs. 9(e) and (h) for $U_{\mathrm{R}} = 10.49$ where chaotic motions start to emerge, and in Figs. 9(f) and (i) for $U_{\mathrm{R}} = 10.95$ where the dynamics of the system is fully chaotic.

5. CONCLUSIONS

The present paper studies the dynamics of two variants of cantilevered flexible plates in axial flow: with an additional (i) spring support and (ii) concentrated mass, with different magnitudes and at various locations along the length of the plate. It has been shown that both the magnitude and the location of the additional spring support or concentrated mass may qualitatively altered the dynamics of the system.

6. ACKNOWLEDGMENT

The leading author is supported by the Open Research Fund Program of Hubei Provincial Key Laboratory of Fluid Machinery and Power Engineering Equipment, and a Natural Sciences and Engineering Research Council of Canada (NSERC) Post-Doctoral Fellowship.

7. REFERENCES

Allen, J.J., Smits, A.J., 2001, Energy harvesting eel. In *Journal of Fluids and Structures* **15**: 629-640.

Dowell, E.H., 1975. *Aeroelasticity of Plates and Shells*. Leyden: The Netherlands.

Kornecki, A., 1978, Aeroelastic and hydroelastic instabilities of infinitely long plates I. In *SM Archives* **3**: 381-440.

Tang, L., Païdoussis, M.P., 2007, On the instability and the post-critical behavior of two-dimensional cantilevered flexible plates in axial flow. In *Journal of Sound and Vibration* **305**: 97-115.

Triantafyllou, M.S., Techet, A.H., Hover, F.S., 2004, Review of experimental work in biomimetic foils. In *IEEE Journal of Oceanic Engineering* **29**: 585-594.

Watanabe, Y., Isogai, K., Suzuki, S., Sugihara, M., 2002b, An theoretical study of paper flutter. In *Journal of Fluids and Structures* **16**: 543-560.